Respiratory and cardiac motion correction in PET using elastic motion approach for simultaneous abdomen and thorax PET/MRI.

Adam Farag (adam.farag@uhn.ca)
UHN: University Health Network https://orcid.org/0000-0002-8439-9498
Joshua Schaefferkoetter
Siemens Medical Solutions USA Inc: Siemens Healthcare USA
Andres Kohan
UHN: University Health Network
Inki Hong
Siemens Medical Solutions USA Inc: Siemens Healthcare USA
Judson Jones
Siemens Medical Solutions USA Inc: Siemens Healthcare USA
Teodor Stanescu
PMH: Princess Margaret Hospital Cancer Centre
Kate Hannemann
UHN: University Health Network
Gonzalo Sapisochin
UHN: University Health Network
Ivan Young
UHN: University Health Network
Ur Metser
UHN: University Health Network
Patrick Veit Haibach
UHN: University Health Network

Research Article

Keywords: Motion correction, PET/MRI, eMOCO

Posted Date: March 30th, 2022

DOI: https://doi.org/10.21203/rs.3.rs-1440002/v1

Version of Record: A version of this preprint was published at Quantitative Imaging in Medicine and Surgery on April 17th, 2023. See the published version at https://doi.org/10.21037/qims-22-1017.

Abstract

Background:

Cardiac and respiratory motions in clinical positron emission tomography (PET) is a major contributor to inaccurate PET quantification and lesion characterisation. In this study, an elastic motion-correction (eMOCO) technique based on mass preservation optical flow is adapted and investigated for PET/MR applications.

Methods:

The eMOCO technique was investigated in a motion management QA phantom and in twenty-four patients who underwent PET/MR for dedicated liver imaging and nine patients for cardiac PET/MR evaluation. Data were acquired and then reconstructed with different gating modes and motion correction techniques and compared to static images. Standardized uptake value (SUV), signal-to-noise ratio (SNR) of lesions activities from each gating mode and correction technique were measured and there means/standard deviation (STD) were compared using 2-ways ANOVA analysis and post-hocTukey's test.

Results:

Lesions' s SNR are highly recovered from phantom and patient studies. The STD of the SUV resulted from the eMOCO technique was statistically significantly less ($p<0.01$) than the STD resulted from conventional gated and static SUVs at the liver, lung and heart.

Conclusions:

The eMOCO technique was successfully implemented in PET/MR imaging in a clinical setting and produced the lowest STD compared to gated and static images, and hence provided the least noisy PET images. Therefore, the eMOCO technique can potentially be used on PET/MRI for improved respiratory and cardiac motion correction.

Introduction

Involuntary motion caused by breathing and cardiac motion are a significant subject of interest and methods for robust correction in routine clinical settings, and are under constant development. In positron emission tomography (PET) imaging, such motions introduce artificial quantities of radioactive tracers in regions of interest (i.e. from image blurring) and hence, result in inaccurate quantification of the standardized uptake value (SUV)[1,2]. Furthermore, for imaging of the abdomen organs such as the liver, respiratory motion can result in incomplete characterization of lesions and may limit lesion detectability[3]. Both types of motions are periodic/quasiperiodic and can at least partly be addressed with appropriate tracking surrogate/controlling techniques[4]. Although respiratory motion can be controlled by breath-hold strategy, it is not suitable for partly minutes-long PET acquisitions[5,6]. The alternative strategy is respiratory tracking and gating in which hardware[7] or software[8] are normally utilized to monitor and/or predict cardiac and respiratory motion models.

In hybrid imaging systems such as PET-computed tomography (PET/CT) respiratory motion correction is particularly challenging as their images are collected sequentially and hence, one of the modalities, or both, are used for motion modelling and correction. For step-and-shoot mode, CT-based motion modeling techniques such as gated 4D-CT[9] and synthetic gated CT from a single frame[10,11] can be used for correction during the reconstruction of PET images. However, such a techniques require longer acquisition time[12] and result consequently in a higher radiation dose[13], and may also suffer from increased noise[14]. Both, noise and increased dose can be addressed in PET-data driven optical flow algorithm, by calculating an elastic transformation between two images based upon the mass conservation of total activities in the field of view (FOV)[15]. With the introduction of both, continuous bed motion (CBM) whole-body PET/CT systems and the elastic motion correction (eMOCO), a clinically useful reduction in noise was achieved[16,17].

However, for hybrid PET-magnetic resonance imaging (PET/MRI) modality, few successful techniques have been introduced to generate cardiac and respiratory motion models including using pulse sequences[18–20], radio frequency (RF) signal[21], and optical tracking. Some of these techniques utilized i.e. 2D-multi-slice T1-Weighted MR Imaging[20], or a 3-D radial stack-of-stars spoiled gradient-echo sequence to generate a set of 3-D volumes for the respiratory cycle phases[22]. Although these techniques may generate satisfying motion models, there is a fundamental trade-off between the potentially improved resolution and increased noise. Therefore, it is necessary to invest in more advanced methods for quantifying the organ motion with less processing time and noise.

Our aim was to 1) implement the eMOCO technique on a PET/MRI, 2) to test and compare the technique in a moving phantom in static and gated techniques to establish ground truth data and 3) to evaluate how such phantom data translate into clinical PET/MR images with different dosage and motion scenarios.

Materials And Methods

Phantom measurements

All phantom and in-vivo image acquisitions in this study were performed on a 3.0T PET/MRI system (Biograph mMR Software Version VE11P, Siemens Healthineers, Erlangen, Germany).

A Zeus MRgRT motion management QA phantom (CIRS, Norfolk, VA) was used to perform the 4D PET/MRI measurements – see Fig. 1. The phantom consists of a fixed body that has a central opening to allow a cylindrical insert to translate and rotate, relative to its axis to generate 1D and 4D motion respectively. The motion actuator consists of two piezoelectric motors and electronics encased in a non-ferromagnetic housing free of RF noise when operated. The motion is applied via a rigid piston to the cylindrical insert. The 4D phantom comes with an application software which allows the user to program the motion with a pre-defined waveform selected from a library or to import a user-defined trace.

Phantom preparation

The phantom's insert and its compartment can be filled with materials to provide MR and/or PET imaging contrast. For the here presented study, the cylindrical insert container in is considered as hot lesion/hot surrounding, whereas the tracking target compartment (0.25 ml volume) represents a cold lesion. The insert was filled with two 18F-FDG concentrations of 45.2 MBq and 11.2 MBq, to simulate normal dose and low dose imaging respectively. In each case, the tracking target was left without any activity to represent a cold lesion.

Phantom PET acquisition

Two breathing rates (16 and 30 breath/min, to simulate normal breathing vs. accelerated breathing) were selected to examine the response of the technique to different breathing rates. The static PET images were acquired first for the normal dose simultaneously with the MRI followed by a gated acquisition for 5min for each breathing rate. A similar set of this PET acquisitions were repeated with the low-dose scenario.

Phantom Data Processing/Reconstruction

All PET data were normalized and corrected for attenuation, scatter, dead-time, and decay time. The full/reduced activity phantom derived PET images were reconstructed as static, respiratory gated and eMOCO corrected data. All PET images were reconstructed using ordinary Poisson ordered-subsets expectation maximization (OP-OSEM)[23] with 3 iterations and 21 subsets using a Gaussian post filter with full width at half-maximum (FWHM) of 4 mm.

Patient measurements

Overall, 24 patients with dedicated PET/MR liver imaging were evaluated. Evaluation of background liver parenchyma, cold as well as hot liver lesions was derived from this data set. Also, background lung measurements were evaluated in these patients. Additionally, nine patients with dedicated cardiac PET/MR imaging were evaluated. All patients underwent PET/MR for different study purposes and not solely for the purpose of motion correction evaluation (REB-ID 16-6123 and 17-6065).

Patient PET/MR acquisition

Patients underwent PET/MR scans 60 minutes after the administration of 18F-FDG, with mean injected activity of 4.8 ± 0.5 MBq/kg. This was followed by simultaneous PET/MRI scan of the abdomen and lung, with PET scan was in the order of 10min. An ANZAI pressure belt (ANZAI Medical Co., LTD, Tokyo, Japan) was attached to the patient's waist to track respiratory phase and amplitude, while the cardiac cycle was tracked via electrocardiograph (ECG).

MRAC was performed using the vendor's standard 2-point Dixon (3D dual-echo spoiled gradient sequence) for all patients. Other study specific sequences which were acquired for the patient studies were not further evaluated for this trial.

Patient Data Processing/Reconstruction

Similar to the phantom study, all PET image were reconstructed utilizing OP-OSEM. For patient image reconstruction and in order to evaluate the performance of the eMOCO and gated techniques with respiratory (RG), cardiac (CG) or dual (DG) gating modes, reconstructions were performed on the same PET data set and binning of the data was performed according to the desired gating mode. This resulted into three corrected PET image sets (representing three gating modes) for each correction technique that allowed observation of the effect of each gating mode and correction technique independently.

Gated correction

Using physiological triggers (ANZAI belt and ECG), the PET data were retrospectively binned. The resulted gated PET-data are used to perform the motion correction. The full/reduced activity image at maximum 'expiration' is treated here as the static case and is compared to that of a single reference gate. The total distribution is "motion deblurred" to match that of the gate. The result is an image with the motion frozen (matching the single gate) but the noise properties of the full count dataset.

eMOCO correction

The eMOCO algorithm was implemented in the e7-toolbox (Siemens Molecular Imaging, Knoxville, USA)[24] and was used to correct the PET-data in phantom as well as patient data retrospectively. The technique produces a single deblurring kernel from the reference frame using the concept of mass preservation approach and applied to each gate as the motion model for respective correction[17]. This model based on the mass preservation optical flow is independent from the motion vectors corresponding to detectable physical motion.

For the purpose of reporting, hot as well as cold liver lesions were evaluated, and the normal liver was considered as the background. Predefined spheres (1, 2 and 3 cm^3), acting as volumes-of-interest (VOIs), were selected for measurements of the liver lesions (for hot and cold lesions) and for lung background measurements (3 cm^3), left ventricle wall measurements (LVW), apex and septum measurements (1 cm^3), and left ventricle cavity measurements (2 cm^3). Different cardiac cycles (1 systole, 8 diastole and 4 in between) were chosen to perform the quantitative measurements to evaluate the effect of the cardiac cycle on the motion correction efficiency. The mean and standard deviation of the SUV at the VOIs were measured for each motion-correction technique and gating mode. To assess the performance of the eMOCO, measurements of the signal-to-noise ratio (SNR) and SUV for static and motion-corrected techniques were performed on PET images and compared.

Statistical analysis

The SUV mean and STD were analysed for static case as well as the motion-correction techniques, gated, and eMOCO, at different gating modes RG, CG and DG. For this analysis, a two-way ANOVA was employed while considering gating mode and reconstruction techniques as the two factors, and is followed by a post-hoc Tukey's honestly significant difference (HSD) test to identify the significance between pairs of means or STD.

Results

Phantom study

The mean SUV and STD measured from the phantom data at low and high doses at different breathing rate are reported in Table 1. The mean SUV derived from eMOCO reconstruction for both breathing rates and for both, low and high doses, were found to be lower than the mean SUV measured in static images, as seen in Fig. 2-a. The respective STDs for these measurements are seen in Table 1-a. The eMOCO provided lowest STD in all settings. Measurements of SNR in the cold lesion of the phantom are demonstrated in Fig. 2-b. Here, the SNR of eMOCO was found to be partly less than the SNR of the static measurement. The ratio between low/high dose concentration, within the phantom was found to be comparable to the ratios between low/high counts in all correction techniques, (Table 1-b).

Table 1
a: Mean SUV ± STD of region selected at the phantom cold lesion, and measured from motion-corrected PET images utilizing gated, and eMOCO techniques at 16 and 30 breathing rates. The measurements were performed for low and high doses.

	breath/min	Static	Gated	eMOCO
low	16	1.09 ± 0.59	0.76 ± 0.39	0.76 ± 0.27
	30	1.12 ± 0.62	1.05 ± 0.34	0.90 ± 0.32
High	16	4.79 ± 1.67	3.52 ± 1.60	3.13 ± 0.92
	30	5.07 ± 2.34	4.87 ± 3.29	4.03 ± 2.17

Table 1
b: Low/high ratio concentration of the phantom and for counts measured for each motion correction technique at both simulated breathing rates. The counts ratio for eMOCO at 16 breath/min is matching the concentration ratio.

Low-to-High dose concentration ratio	breath/min	Low-to-High counts ratio		
0.248		Static	Gated	eMOCO
	16	0.228	0.216	0.244
	30	0.221	0.207	0.225

Patient studies

Background measurements from 552 lower right lung, 458 middle right lung and 493 superior right lung (Fig. 3) were analysed for static, gated and eMOCO reconstructions. Similarly for the liver, 1303 liver segments were used for background SUV measurements and analyses and overall 9 hot (FDG avid) liver lesions and 24 cold liver lesions were measured. For the heart, 386 septum regions and 392 LVW regions were used in the analysis. The global mean SUV (summarizing all measured ROI's) and STD measured from the selected regions for static and motion correction techniques in each gating mode are reported in Table 2.

Table 2
Global mean SUV ± STD of regions selected in liver and lung and measured from motion-corrected PET images utilizing gated, and eMOCO techniques. An equivalent mean or lower STD is shown for eMOCO compared to the gated reconstruction is shown throughout different gating modes (respiratory, cardiac and dual gating).

		RG	CG	DG
Static	liver	2.09 ± 0.18	2.23 ± 0.22	-
	lung	0.44 ± 0.10	0.42 ± 0.08	-
	Septum	8.86 ± 0.56	8.86 ± 0.56	8.86 ± 0.56
	LVW	12.92 ± 1.63	12.92 ± 1.63	12.92 ± 1.63
Gated	liver	2.18 ± 0.30	2.30 ± 0.61	2.28 ± 0.99
	lung	0.47 ± 0.12	0.48 ± 0.17	0.48 ± 0.27
	Septum	8.02 ± 1.22	9.04 ± 1.34	9.96 ± 2.08
	LVW	13.58 ± 0.93	13.23 ± 1.85	13.47 ± 1.55
eMOCO	liver	2.17 ± 0.23	2.20 ± 0.31	2.12 ± 0.39
	lung	0.46 ± 0.09	0.47 ± 0.10	0.47 ± 0.10
	Septum	8.36 ± 1.00	9.16 ± 1.20	9.68 ± 1.16
	LVW	14.70 ± 1.27	13.88 ± 2.20	14.58 ± 1.52

The global mean SUV for lung and liver background measurements showed that the performance for gated and eMOCO reconstruction are comparable or partly improved by the eMOCO reconstruction.

Liver Measurements

The SNR measured in cold lesions and hot background measurements in images (Fig. 4) produced by gated techniques were significantly lower ($p = 0.012$) than those obtained from images reconstructed using eMOCO technique. The SNR measured at the cold lesion for patients' data followed a similar pattern to the SNR measured in the phantom's cold lesion (Fig. 2-b).

The two-factor ANOVA analysis of the mean SUV's shows no statistically significant differences between motion correction techniques and the static reconstruction (Table 3). There was also no statistical interaction/dependency between the type of gating and the applied motion correction technique. However, again for STDs there were significant differences found (Table 3). Furthermore, an interaction/dependency between type of gating and technique of motion-correction was found (Table 3, $F(4,162) = 42.96$, $p < 0.01$). Although the mean SUV for eMOCO was comparable to gated reconstruction, the STD was significantly lower ($p < 0.05$) compared to the gated technique when cardiac and dual gating modes are used. They are however not statistically significantly different when using respiratory gating.

Table 3
Two-factor ANOVA testing results of motion-correction techniques and gating modes in liver, lung and heart measurements. The mean SUV and STD at the heart are showing partly significant differences and dependency between the gating mode and the motion-correction technique.

		Liver	Lung	Heart
Mean SUV	gating mode	(F(2,162) = 0.17, p = 0.84)	**(F(2,162) = 930.90, p < 0.01)**	**(F(2,216) = 86.99, p < 0.01)**
	Motion-correction techniques	(F(2,162) = 0.12, p = 0.89)	(F(2,162) = 0.83, p = 0.44)	**(F(2,216) = 87.55, p < 0.01)**
	interaction	(F(4,162) = 0.40, p = 0.81)	(F(4,162) = 2.28, p = 0.06)	**(F(4,216) = 14.00, p < 0.01)**
STD	gating mode	**(F(2,162) = 60.41, p < 0.01)**	**(F(2,162) = 28.371, p < 0.01)**	**(F(2,216) = 155.75, p < 0.01)**
	Motion-correction techniques	**(F(2,162) = 180.61, p < 0.01)**	**(F(2,162) = 56.51, p < 0.01)**	**(F(2,216) = 162.62, p < 0.01)**
	interaction	**(F(4,162) = 42.96, p < 0.01)**	**(F(4,162) = 13.68, p < 0.01)**	**(F(4,216) = 36.38, p < 0.01)**

Figure 5 shows example images for lung and liver background in case of static, and both, the gated and eMOCO reconstruction techniques. It is apparent that noise from eMOCO image is lower than the static and gated images.

Heart Measurements

Overall, mean SUV and STD measured in the heart VOI's reconstructed with eMOCO, gated and static were statistically significantly different. There were also significance dependences in the mean SUV's of the motion-correction techniques and the gating modes (Table 3).

Post-hoc Tukey's HSD testing

The results from the post-hoc Tukey's HSD with studentized range statistic (Q-statistic) for liver measurements is shown in Fig. 6-a, the corresponding HSD p-values are shown in Table 4. The most significant differences of the mean SUV and STD are seen in static vs gated reconstruction ($p < 0.01$) and gated reconstruction vs eMOCO ($p < 0.01$) when CG or DG techniques are applied.

Table 4
Post-hoc Tukey test results of measured mean SUV in liver, lung and heart images, which were reconstructed with different motion correction techniques and gating modes. * Indicates phase (4) in-between systole and diastole, while ** indicates systole phase (1).

		Liver			Lung			Heart			Septum *		LVW **	
		RG	CG	DG	RG	CG	DG	RG	CG	DG	CG	DG	CG	DG
Mean SUV	Static vs Gated	0.900	0.816	0.357	0.471	0.001	0.001	0.284	0.001	0.001	0.007	0.015	0.536	0.476
	Static vs eMOCO	0.900	0.200	0.573	0.770	0.001	0.001	0.234	0.001	0.001	0.029	0.044	0.012	0.006
	Gated vs eMOCO	0.900	0.487	0.900	0.845	0.900	0.452	0.900	0.900	0.900	0.726	0.821	0.098	0.069
STD	Static vs Gated	0.205	0.001	0.001	0.181	0.001	0.001	0.120	0.001	0.001	0.003	0.001	0.842	0.900
	Static vs eMOCO	0.863	0.900	0.052	0.803	0.021	0.026	0.253	0.001	0.001	0.012	0.098	0.357	0.900
	Gated vs eMOCO	0.441	0.001	0.001	0.463	0.034	0.001	0.900	0.590	0.001	0.724	0.011	0.654	0.900
	insignificant	$p < 0.05$	$p < 0.01$											

The post-hoc Tukey's HSD test showed that the mean SUV for static vs gated reconstruction and static vs eMOCO reconstruction are significantly different when using cardiac gating in lung and heart measurements ($p < 0.01$), while this is not the case for gated vs eMOCO as seen in Table 4.

Discussion

Elastic motion correction (eMOCO) is usually used in PET/CT to correct for cardiac and respiratory motions in PET images, which has proven to be effective[24–26].

In this study, we implemented the eMOCO technique on a PET/MRI system and investigated its performance in a phantom as well as clinical setting. The main finding from this study is that the eMOCO improved the STD in different reconstruction and thereby provided lower noise levels within the images. The phantom results suggest that eMOCO would not necessarily improve the SNR in cold lesions. However, it may still improve detectability since the SNR at cold lesion is not necessarily correlated to detection performance as it is with hot lesions.

The statistical analysis of the hot lesions within the liver presented no significant differences between the mean SUV, however the STD from eMOCO images was found to be statistically significantly lower when compared with the gated techniques. This indicates that the eMOCO enables PET-images with less statistical noise compared to the standard clinical gating technique. The lower STD in images corrected by eMOCO was apparent in liver, lung and heart VOIs measurements and in particular when cardiac and dual gating was applied. This suggests a dependency of the cardiac and dual gating modes on the correction technique. One explanation is that the eMOCO algorithm, when applied to all phases of the cardiac cycle (8 phases), includes the counts of all cardiac gates into the reference gate[24].

From a clinical/practical perspective, the here found advantages of the eMOCO might not be as impressive as initially anticipated, at least not within our group. However, the specific improvements which have been found are nevertheless important for clinical reading. First of all, the fact that the results from the phantom measurements are translated into patient imaging findings speaks for the robustness of the method. The results, namely the partly reduced noise/increased SNR are important for clinical reading as it provides the radiologist/imaging reader with increased accuracy for quantification. This is especially important in follow up studies where clinical decisions are dependent of accurate measurement of differences or quantification of lesions. Many therapy decision criteria are now based on measurement of ratio's (i.e. Deauville Criteria for lymphoma or myeloma, Hopkins Criteria for Head and Neck cancer, PROMISE score for PSMA imaging or Krenning Score for neuroendocrine tumour imaging). The partly increased consistency and reduction of standard deviation provided by the eMOCO compared to other reconstruction methods is offering additional accuracy for those specific clinical scenarios.

There are several strategies to achieve PET motion compensation within PET/MRI. The core requirement for a given strategy is an accurate respiratory motion model that can be generated with either the aid of external device (belt), MR data or PET data. Common MR-based respiratory motion models such as retrospective gating and averaging over multiple respiratory cycles[27] usually provide better image quality but are unable to reflect inter-cycle variations in the respiration pattern. Another MR-based motion model can be generated using fast MR pulse sequences, but images may suffer loss of signal-to-noise ratio and decreased spatial resolution. While, MR-based MOCO techniques can be applied to PET data using either motion compensated image reconstruction (MCIR)[27] or post-reconstruction registration (PRR)[28], they usually require specific modified pulse sequence in place, and/or performing MRI scanning throughout the whole PET acquisition time. One example of these techniques is the BodyCompass™[29–31] which utilizes a 3D T1-weighted radial stack-of-stars MRI pulse sequence to calculate the respiratory signal and create the motion model. In this sequence, the respiratory signal is acquired during the full PET acquisition in order to preserve both high spatial resolution and the different respiratory pattern. The technique does not require navigator echo nor external devices as a source of motion signal, instead, self-gating in a retrospective PRR reconstruction fashion is utilized. The drawback of this technique is the need for optimization of number of bins and bin sizes which are required to reduce the intra-bin motion at the diaphragm. Additionally, to generate a sufficient motion model in this case, relatively long scan time is also required which subsequently may thwarts useful MRI information during this time. It is worth mentioning here that BodyCompass was not reported in this study, since it could not be implemented with phantom acquisitions.

In contrast to self-gated MR-based MOCO, PET-based eMOCO, reported in this study, depends only on the sensor that provides the motion information while utilizing the PET data itself without the dependency on inputs from the MR side. This allowed the use of the PET-data fully without the loss of information from both MRI and PET modalities. The eMOCO algorithm computation time was also tolerable to a clinical setting which is an advantage in terms of the complete reconstruction time. Overall eMOCO is partly significantly better in phantom measurements, in breathing type motion corrections, even with lower doses – overall offering several advantages for those type of acquisitions. This was found to partly even true for cardiac imaging.

The decision on which technique to be used for motion correction still depends on the availability of the algorithms used in motion model generation and correction, as well as and the scanner time. In our study we were able to perform the eMOCO technique with the aid of offline reconstruction-eMOCO combined algorithm which required specific setting that is not yet available for clinical routine. Implementation of the eMOCO into the PET/MRI modality still to be achieved before it is available for all studies.

Conclusion

In conclusion, the elastic motion correction technique partly significantly reduced STD in PET measurements and thereby reduces noise compared to the static and gated datasets. Thus, overall improved quantification of lesions can be enabled by this technique. The eMOCO technique is a viable option for partly improved respiratory and cardiac motion correction method and appears to be suitable for a clinical setting.

Abbreviations

eMOCO
Elastic motion correction
PET
Positron emission tomography
MRI
Magnetic resonance imaging
CT
computed tomography
RG
respiratory gating
CG
cardiac gating
DG
dual gating
VOI
volume of interest
FDG
18F-Fluoro-deoxy-glucose
FOV
Field-of-view
RF
Radio frequency
SUV
Standardized uptake value
SNR
Signal-to-noise ratio
STD
Standard deviation
OP-OSEM
3i-24s Ordinary Poison estimation method.

Declarations

Authors' contributions

Both JS and AF share first authorship of this manuscript. JS contributed in phantom data acquisition, examination, processing and editing the manuscript. AF contributed in data examination, processing, statistical analysis, and writing and editing the manuscript. AK, contributed in processing VOIs measurements and editing the manuscript. IH and JJ provided the motion correction algorithm used in this study. TS planned the phantom acquisition and editing the manuscript. KH, GS, IY and UM edited the manuscript. PVH examined the data and contributed in writing and editing the manuscript. The authors read and approved the final manuscript.

Ethics approval and consent to participate

Informed consent was obtained from patients involved in this study. All procedures performed were in accordance with the research ethics protocol approved by the University Health Network, REB-ID 16-6123 and 17-6065.

Consent for publication

There is no identifying information about participants in this study. Consent for publication was obtained from each participant before inclusion into the study.

Availability of data and material

The data that support the findings of this study are available from University Health Network, but restrictions apply to the availability of these data, which were used under license for the current study and so are not publicly available. Data are however available from the authors upon reasonable request and with permission of University Health Network.

Competing interests

JS, IH and JJ are full time employees of Siemens Healthcare. The rest of the authors declare that they have no competing interest.

Funding:

Not applicable

Acknowledgments:

Not applicable

Complementory data

Lung Measurements

A sample of patient-derived lung PET images produced by the static-, gated and eMOCO techniques are shown in figure 5 – here, the noise level in the eMOCO reconstruction appears to be much lower than the gated images. The mean SUV were found not to be statistically significant different between static, gated and eMOCO, while the two-way ANOVA test shows significant differences (see Table 3, $F(2,162) = 930.9$, $p = p<0.01$) in the mean SUV (when applying different gating modes). Similar to the liver results, the two-way ANOVA test on the STD showed significant differences between the motion-correction techniques (Table 3, $F(2,162) = 56.51$, $p<0.01$), as well as the gating modes (Table 3, $F(2,162) =28.37$, $p<0.01$).

References

1. Osman MM, Cohade C, Nakamoto Y, Wahl RL. Respiratory motion artifacts on PET emission images obtained using CT attenuation correction on PET-CT. Eur J Nucl Med Mol Imag. 2003;30(4):603–6.
2. Erdi YE, Nehmeh SA, Pan T, et al. The CT motion quantitation of lung lesions and its impact on PET-measured SUVs. J Nuclear Med. 2004;45(8):1287–92.
3. Li G, Schmidtlein CR, Burger IA, Ridge CA, Solomon SB, Humm JL. Assessing and accounting for the impact of respiratory motion on FDG uptake and viable volume for liver lesions in free-breathing PET using respiration-suspended PET images as reference. Med Phys. 2014;41(9):091905.
4. Gillman A, Smith J, Thomas P, Rose S, Dowson N. PET motion correction in context of integrated PET/MR: Current techniques, limitations, and future projections. Med Phys. 2017;44(12):e430–45.
5. Nagamachi S, Wakamatsu H, Kiyohara S, et al. Usefulness of a deep-inspiration breath-hold 18F-FDG PET/CT technique in diagnosing liver, bile duct, and pancreas tumors. Nuclear Med Commun. 2009;30(5):326–32.
6. Raper AJ, Richardson D, Kontos H, Patterson J Jr. Circulatory responses to breath holding in man. J Appl Physiol. 1967;22(2):201–6.
7. Bailey DL, Kalemis A. Externally triggered gating of nuclear medicine acquisitions: a useful method for partitioning data. Phys Med Biology. 2005;50(7):N55.
8. Werner MK, Parker JA, Kolodny GM, English JR, Palmer MR. Respiratory gating enhances imaging of pulmonary nodules and measurement of tracer uptake in FDG PET/CT. Am J Roentgenol. 2009;193(6):1640–5.
9. Pönisch F, Richter C, Just U, Enghardt W. Attenuation correction of four dimensional (4D) PET using phase-correlated 4D-computed tomography. Phys Med Biology. 2008;53(13):N259.
10. McQuaid SJ, Lambrou T, Hutton BF. A novel method for incorporating respiratory-matched attenuation correction in the motion correction of cardiac PET–CT studies. Phys Med Biology. 2011;56(10):2903.
11. Fayad H, Lamare F, Bettinardi V, Roux C, Visvikis D. Respiratory synchronized CT image generation from 4D PET acquisitions. Paper presented at: 2008 IEEE Nuclear Science Symposium Conference Record2008.
12. Allen-Auerbach M, Yeom K, Park J, Phelps M, Czernin J. Standard PET/CT of the chest during shallow breathing is inadequate for comprehensive staging of lung cancer. J Nuclear Med. 2006;47(2):298–301.

13. Nye JA, Esteves F, Votaw JR. Minimizing artifacts resulting from respiratory and cardiac motion by optimization of the transmission scan in cardiac PET/CT. Med Phys. 2007;34(6Part1):1901–6.
14. Souvatzoglou M, Bengel F, Busch R, et al. Attenuation correction in cardiac PET/CT with three different CT protocols: a comparison with conventional PET. Eur J Nucl Med Mol Imag. 2007;34(12):1991–2000.
15. Dawood M, Gigengack F, Jiang X, Schäfers KP. A mass conservation-based optical flow method for cardiac motion correction in 3D-PET. Med Phys. 2013;40(1):012505.
16. Hong I, Jones J, Hamill J, Michel C, Casey M. Elastic motion correction for continuous bed motion whole-body PET/CT. Paper presented at: 2016 IEEE Nuclear Science Symposium, Medical Imaging Conference and Room-Temperature Semiconductor Detector Workshop (NSS/MIC/RTSD)2016.
17. Hong I, Jones J, Casey M. Ultrafast elastic motion correction via motion deblurring. Paper presented at: 2014 IEEE Nuclear Science Symposium and Medical Imaging Conference (NSS/MIC)2014.
18. Munoz C, Neji R, Cruz G, et al. Motion-corrected simultaneous cardiac positron emission tomography and coronary MR angiography with high acquisition efficiency. Magn Reson Med. 2018;79(1):339–50.
19. Kolbitsch C, Prieto C, Tsoumpas C, Schaeffter T. A 3D MR-acquisition scheme for nonrigid bulk motion correction in simultaneous PET-MR. Med Phys. 2014;41(8Part1):082304.
20. Würslin C, Schmidt H, Martirosian P, et al. Respiratory motion correction in oncologic PET using T1-weighted MR imaging on a simultaneous whole-body PET/MR system. J nuclear Med. 2013;54(3):464–71.
21. Han F, Rapacchi S, Hu P. Prospective cardiac motion self-gating. Quant imaging Med Surg. 2017;7(2):215.
22. Grimm R, Fürst S, Dregely I, et al. Self-gated radial MRI for respiratory motion compensation on hybrid PET/MR systems. Paper presented at: International Conference on Medical Image Computing and Computer-Assisted Intervention2013.
23. Comtat C, Bataille F, Michel C, et al. OSEM-3D reconstruction strategies for the ECAT HRRT. Paper presented at: IEEE Symposium Conference Record Nuclear Science 2004.; 16–22 Oct. 2004, 2004.
24. Bellinge JW, Majeed K, Carr SS, et al. Coronary artery 18F-NaF PET analysis with the use of an elastic motion correction software. Journal of Nuclear Cardiology. 2019:1–10.
25. Pösse S, Büther F, Mannweiler D, et al. Comparison of two elastic motion correction approaches for whole-body PET/CT: motion deblurring vs gate-to-gate motion correction. EJNMMI Phys. 2020;7(1):1–14.
26. Meier JG, Wu CC, Cuellar SLB, et al. Evaluation of a novel elastic respiratory motion correction algorithm on quantification and image quality in abdominothoracic PET/CT. J Nuclear Med. 2019;60(2):279–84.
27. Ouyang J, Li Q, El Fakhri G. Magnetic resonance-based motion correction for positron emission tomography imaging. Paper presented at: Seminars in nuclear medicine2013.
28. Chun SY, Reese TG, Ouyang J, et al. MRI-based nonrigid motion correction in simultaneous PET/MRI. J Nuclear Med. 2012;53(8):1284–91.
29. Grimm R, Fürst S, Souvatzoglou M, et al. Self-gated MRI motion modeling for respiratory motion compensation in integrated PET/MRI. Med Image Anal. 2015;19(1):110–20.
30. Chen Z, Sforazzini F, Baran J, Close T, Shah NJ, Egan GF. MR-PET head motion correction based on co-registration of multicontrast MR images. Wiley Online Library; 2021. pp. 1065–9471.
31. Fürst S, Grimm R, Hong I, et al. Motion correction strategies for integrated PET/MR. J nuclear Med. 2015;56(2):261–9.

Figures

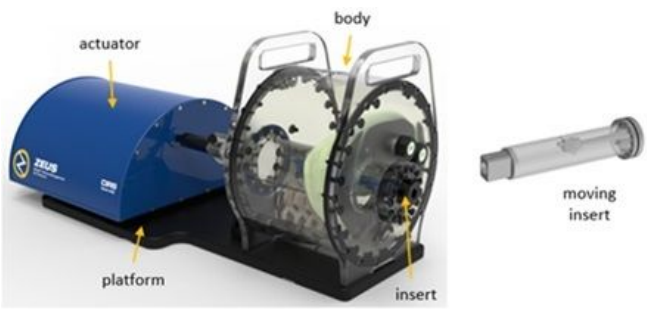

Figure 1

4D phantom used for acquiring the 4D PET-MR data: phantom ensemble including the main body sub-component, a movable cylindrical insert, piston and supporting platform.

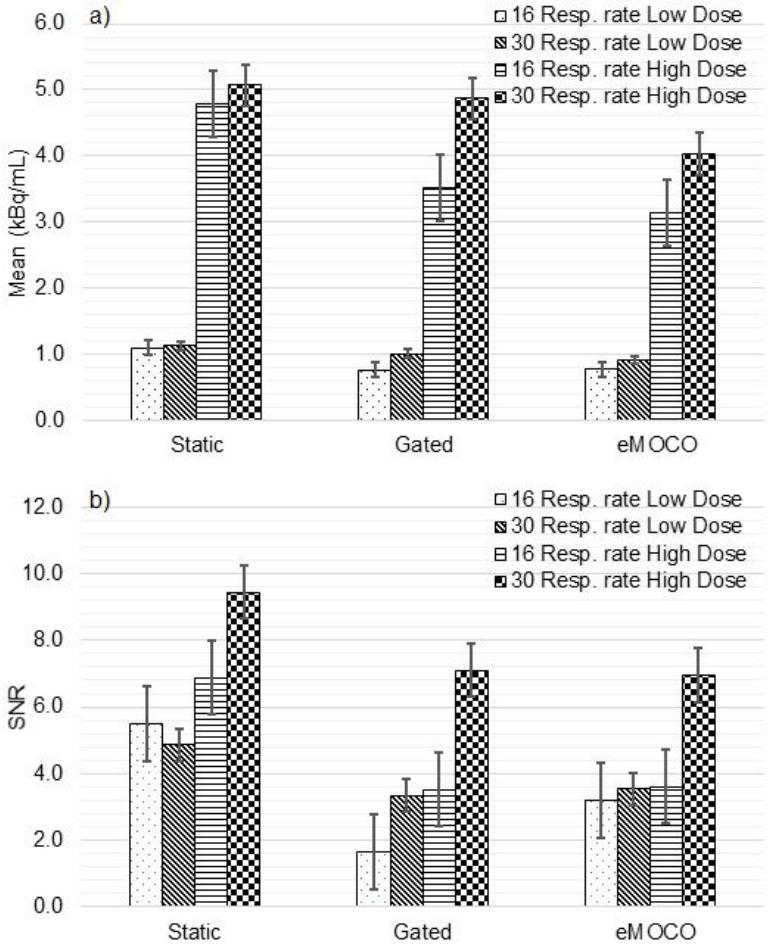

Figure 2

a) Mean activities within the cold lesion of the phantom from motion-corrected images using gated and eMOCO techniques. The mean values from low-dose measurements with 16 and 30 respiration/min are comparable between gated and eMOCO techniques. For high-dose measurements, the mean activities are also comparable between gated and eMOCO, with eMOCO showing the lowest values. b) SNR measured in the cold lesion of the phantom.

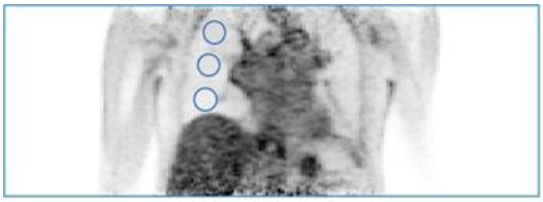

Figure 3

Example PET image of the chest and abdomen showing three blue circled regions of interest in the lung.

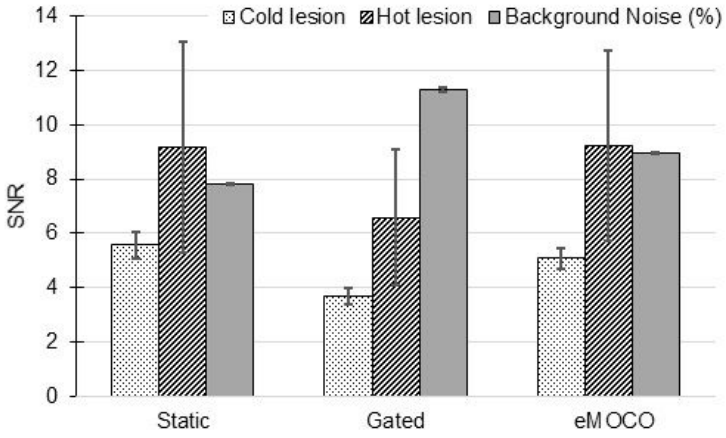

Figure 4

Mean signal-to-noise ratio (SNR) for 5 hot and 7 cold lesions (patients), from motion corrected PET data using gated and eMOCO techniques. Showing also, the percentages of background noise (solid grey bars) for all reconstruction techniques, where percentage noise from eMOCO images are lower compared to the gated technique.

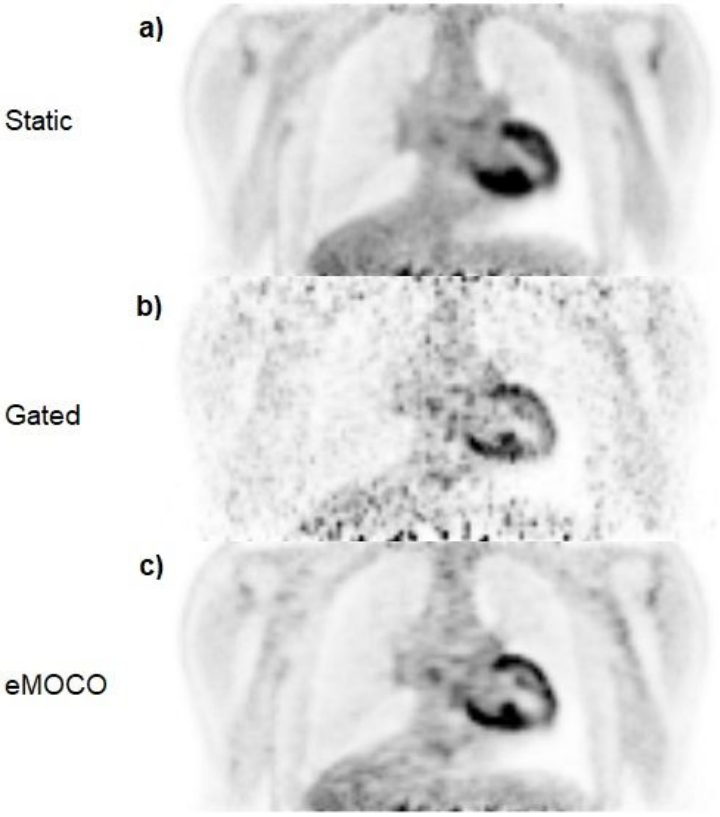

Figure 5

Cardiac motion-corrected PET images showing a) static b) gated and c) eMOCO. Noise level is shown to be higher in gated images than the eMOCO images.

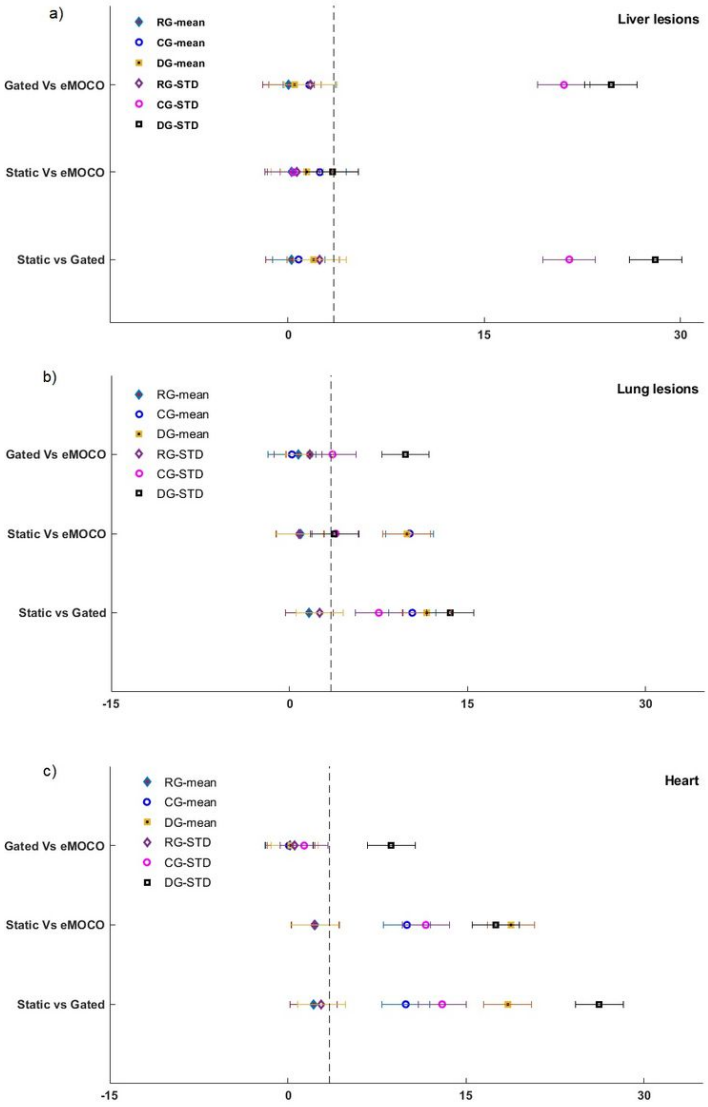

Figure 6

A display of Post-hoc Tukey's HSD Q-statistic results with 3.408 as the cut-off (vertical dashed line) between significant (Q>3.408) and not significant (Q<3.408) differences. The HSD representing the significant differences between the mean SUV, and also the STD, for a pair of reconstruction techniques at different gating modes, respiratory-gating (RG-mean and RG-STD), cardiac-gating (CG-mean and CG-STD), dual-gating (DG-mean and DG-STD), for the regions of the a) liver, b) lung and c) heart. For the liver a), the test shows high significant difference between STD of gated and eMOCO techniques when applying either cardiac gating (CG-STD) or dual gating (DG-STD) modes.